Inorganic Chemistry

pubs.acs.org/IC Article

Introducing Bluish-Green Light-Emitting Diodes (OLEDs) and Tuning Their Color Intensity by Uranium Complexes: Synthesis, Characterization, and Photoluminescence Studies of 8-Hydroxyquinoline Complexes of Uranium

Khodabakhsh Darzinezhad, Mostafa M. Amini,* Mohammad Janghouri, Ezeddin Mohajerani, Mohammad-Reza Fathollahi, Zahra Jamshidi, and Christoph Janiak*

Cite This: *Inorg. Chem.* 2020, 59, 17028−17037 Read Online

ACCESS | Metrics & More | Article Recommendations | Supporting Information

ABSTRACT: To improve our understanding of the chemistry of actinide complexes and to spur their development in the field of actinide markers, two new uranium complexes were synthesized using 8-hydroxyquinoline and 5,7-dichloro-8-hydroxyquinoline. The prepared complexes were characterized by Fourier transform infrared spectroscopy, thermogravimetric analysis, ultraviolet−visible spectroscopy, elemental analysis, and single-crystal X-ray diffraction. The impact of the electron-withdrawing group of the ligand on the photoluminescence spectra of the complexes in solution and in the solid state was scrutinized. The bandgap of the complexes was calculated using the density functional theory (DFT) method to investigate the effects of the electron-withdrawing groups on energy levels. The synthesized uranium complexes demonstrated appropriate levels of the lowest unoccupied molecular orbital energy, leading to favorable dye stability. The prepared uranium complexes showed blue fluorescent emission, and the sample with the most intense fluorescence was used to construct bluish-green organic light-emitting diodes using simple solution processing fabrication methods. Absorbance spectra, emission spectra, DFT-calculated energy levels, and comparisons of the fabricated organic light-emitting diodes indicated that the electron-withdrawing group was a key factor in photoluminescence behavior.

INTRODUCTION

Despite long-lasting developments in the chemistry of actinides (An^{n+}) and actinyls (AnO_2^{n+}), this field is currently undergoing a renaissance of exploration because their various chemical and physical properties, as well as their electronic structure and bonding, yield new insights and applications. The need for comprehensive investigations of actinides, even their known optical properties, has been well acknowledged, especially when compared with their lanthanide counterparts as well as with transition elements. All actinides have optical luminescence properties. The characteristic luminescence of uranium, mainly uranium(VI), has been examined more extensively than those of the other actinides. The photochemical and photophysical properties of uranium-containing compounds are highly significant in diagnostic tests as well as in the manufacture of blue-green glassware and ceramics, internal radiation biochemistry, and optical sensors.[1]

The photoluminescence spectrum of uranium complexes appears as a broad peak in the range of 400−650 nm, and it can be detected with a microsecond lifetime.[2−6] The broad peak, which originates mainly within the uranyl ion, is a result of the transfer of an electron from the oxygen orbital to a vacant uranium 5f orbital.[7,8] The ultraviolet−visible (UV−vis) spectra of uranium complexes have been found to be more complicated when their equatorially coordinated ligands have a π-conjugation system, which then provokes other electronic transitions, including ligand-centered charge transfer. The conjugation system acts as an antenna and facilitates energy transfer; consequently, it influences the fluorescence wavelength by shifting its position.[9,10]

Uranium complexes have different geometrical arrangements. The best-known geometrical structure of uranium is uranyl, which has a linear structure but in the presence of various connectors can form square-bipyramidal, pentagonal-bipyramidal, cubic, hexagonal-bipyramidal, and tricapped

Received: July 29, 2020
Published: November 24, 2020

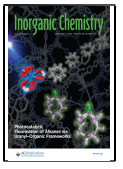

https://dx.doi.org/10.1021/acs.inorgchem.0c02242
Inorg. Chem. 2020, 59, 17028−17037

trigonal prismatic structures in uranium complexes.[11] The uranyl ion has a linear structure, UO_2^{2+}. It is a dioxido cation of uranium in the VI oxidation state. Uranyl is ubiquitously found in the form of salts, including acetate, phosphate, nitrate, perchlorate, sulfate, selenite, iodate, and oxide.[12] The uranyl moiety is also the central part of most uranium complexes, where the organic ligands are then equatorially coordinated in an overall square-, pentagonal-, or hexagonal-bipyramidal fashion.[13,14] Uranium complexes can adopt structures such as monomers, one-, two-, and three-dimensional coordination polymers,[15−23] and metal−organic frameworks (MOFs).[24−30]

Despite the vast number of studies of uranium complexes, there are only a few 8-hydroxyquinoline complexes, and their photoluminescence has not been examined;[31−35] however, this ligand is interesting for the optical properties of most transition metals and lanthanide complexes. The use of depleted uranium (^{238}U) complexes in the lighting industry is highly advantageous over main group metal, transition metal, or lanthanide complexes. On one hand, main group metal complexes usually do not have a high radiation efficiency in commercial applications. On the other hand, iridium and other rare transition metals and lanthanides are trace elements in the Earth's crust. One reason that organic light-emitting diodes (OLEDs) are so expensive at present is the need to use iridium and other rare metals in their manufacture. Because the abundance of uranium is approximately 4000−5000 times higher than that of iridium and other rare metals, its application can have a significant effect on reducing the cost of commercial OLEDs. Moreover, actinides have a much stronger emission intensity than lanthanides.[36] It is expected that the introduction of new compounds of uranium will revolutionize the future lighting market.

Because of the fascinating photoluminescence behavior of 8-hydroxyquinoline complexes of various metals, the syntheses, characterization, and investigation of the optical properties of diverse derivatives of 8-hydroxyquinoline complexes of uranium should prove to be beneficial. In this context, in this study, we used 8-hydroxyquinoline and 5,7-dichloro-8-hydroxyquinoline to synthesize two uranium complexes, $UO_2(C_9H_6NO)_2(CH_3OH)$ (**1**) and $UO_2(C_9H_4NOCl_2)_2(CH_3OH)$ (**2**), and examined the effect of electron-withdrawing chloro substituents of 8-hydroxyquinoline on its photoluminescence behavior.

Because of its many challenges, a blue emitter continues to be a major issue in OLED development.[37] In this study, the prepared complexes were used as pigments to fabricate blue light-emitting diodes employing solution processing methods.[38]

EXPERIMENTAL SECTION

Materials and Instrumentation. Depleted uranyl acetate dihydrate [$^{238}UO_2(acetate)_2{\cdot}2H_2O$], 8-hydroxyquinoline, and 5,7-dichloro-8-hydroxyquinoline were purchased from Merck and Aldrich and used without further purification. All materials for fabrication of the OLEDs, 2,9-dimethyl-4,7-diphenyl-1,10-phenanthroline (BCP), poly(vinylcarbazole) (PVK), 4-(dicyanomethylene)-2-methyl-6-(4-dimethylaminostyryl)-4*H*-pyran (DCM), *N*,*N*′-bis(3-methylphenyl)-*N*,*N*′-diphenylbenzidine (TPD), 2-phenyl-5-(4-biphenylyl)-1,3,4-oxadiazole (PBD), poly(3,4-ethylenedioxythiophene):poly(styrenesulfonate) (PEDOT:PSS), and indium tin oxide (ITO) (see Scheme S1 for structures), were obtained from Aldrich. All solvents were dried and distilled under nitrogen before use according to standard procedures.[39] Melting points were obtained with an Electrothermal 9200 melting point apparatus. Elemental microanalyses (CHN) were performed with a Thermo Finnigan Flash-1112EA CHNS elemental analyzer. Infrared spectra from 4000 to 250 cm^{-1} were recorded on a Bomem MB-series Fourier transform infrared (FTIR) instrument with a spectral resolution of 4 cm^{-1} using KBr pellets of the compounds. Thermogravimetric analysis (TGA) of the complexes was performed using a Bahr STA-503 instrument at a heating rate of 10 °C min^{-1} in air. The photoluminescence spectra were recorded in THF at a concentration of 1.0×10^{-6} mol L^{-1} at room temperature on a PerkinElmer LS-45 luminescence spectrometer by excitation with 350 nm and in the solid state at room temperature by the same excitation wavelength using a JASCO FP-6500 spectrofluorometer. UV−vis spectra were also recorded in a quartz cell with a concentration of 1.0×10^{-4} mol L^{-1} on a Shimadzu 2100 spectrophotometer. The layer thickness was measured with a Dektak8000 profilometer and a Sigma Instrument SQM160 crystal thickness monitor system. The current−voltage characteristics of the fabricated devices were inspected with a Keithley 2400 source measurement unit. A Mastech-MS6612 optical instrument was used to record the emission intensity versus voltage relations of the OLEDs. Finally, the electroluminescence and photoluminescence spectra were recorded on a USB2000 and HR4000 Ocean Optics instrument.

X-ray Crystallography. Single-crystal X-ray measurements were conducted on a Bruker Kappa APEX2 CCD diffractometer with a microfocus tube using Mo Kα radiation (λ = 0.71073 Å) and ω- and φ-scans. Data collection was carried out with APEX2 software; cell refinement and data reduction were performed with SAINT,[40] and experimental absorption correction was performed with SADABS.[41] The structures were determined by direct methods using SHELXT2014/7 and refined by full-matrix least squares of F2 with SHELXL2014/7.[42] Non-hydrogen atom positions were refined with anisotropic displacement parameters. Hydrogen atoms were positioned geometrically (with C−H bond lengths of 0.95 Å for aromatic and aliphatic CH, 0.99 Å for CH_2, and 0.98 Å for CH_3) and riding models (AFIX 43, 23, and 137, respectively), with U_{iso}(H) = 1.2Ueq (CH and CH_2) and 1.5Ueq (CH_3). The hydrogen atoms for the methanol molecules were found from the electron density map. Graphics were drawn with DIAMOND.[43] Crystallographic data and the refinement parameters for $UO_2(C_9H_6NO)_2(CH_3OH)$ (**1**) and $UO_2(C_9H_4NOCl_2)_2(CH_3OH)$ (**2**) are listed in Table S1.

Density Functional Theory (DFT). Density functional theory (DFT) was carried out using the hybrid Perdew−Burke−Ernzerhof (PBE0)[44] exchange-correlation density functional. The accuracy of the PBE0 functional has been recently checked for spectroscopic properties of the uranium compound in comparison to the experiment.[45] The all-electron SARC-ZORA-TZVP,[46] segmented all-electron relativistically contracted (SARC) basis sets with zero-order regular approximation (ZORA)[47] Hamiltonian that consider the scalar-relativistic term, has been used for uranium. For the other elements, the Def2-TZVP (triple-ζ valence basis sets with polarized function)[48] basis set was applied. All calculations were performed using the ORCA4.0 package.[49]

Synthesis of $UO_2(C_9H_6NO)_2(CH_3OH)$ (1). Uranyl acetate dihydrate (0.2 mmol, 0.085 g) [**Caution! $^{238}UO_2(acetate)_2{\cdot}2H_2O$ is toxic and somewhat radioactive**] and 8-hydroxyquinoline (0.4 mmol, 0.058 g) were mixed and sonicated in methanol for 10 min. The mixture was then sealed in a 25 mL glass tube and heated at 85 °C. After 6 days, the tube was cooled to room temperature naturally, and the light-brown crystals were collected, washed with deionized water, dried at room temperature, and used for characterizations (yield of 84.7%, mp >270 °C). Anal. Calcd (found) for $C_{19}H_{16}N_2O_5U$: C, 38.65 (38.80); H, 2.73 (2.46); N, 4.75 (4.98). IR (KBr pellet): 3518, 3431, 3083, 2924, 1623, 1565, 1465, 1383, 1306, 1265, 1101, 1003, 901, 830, 737, 594, 481 cm^{-1}.

Synthesis of $UO_2(C_9H_4NOCl_2)_2(CH_3OH)$ (2). Uranyl acetate dihydrate (0.2 mmol, 0.085 g) and 5,7-dichloro-8-hydroxyquinoline (0.4 mmol, 0.086 g) were mixed and sonicated in methanol. After being mixed for 10 min, the mixture was then sealed in a 25 mL glass tube and heated at 85 °C. After 6 days, the tube was cooled to room temperature naturally, and the dark-brown crystals were collected,

https://dx.doi.org/10.1021/acs.inorgchem.0c02242
Inorg. Chem. 2020, 59, 17028−17037

washed with ultrapure water, dried at room temperature, and used for characterizations (yield of 89.3%, mp >270 °C). Anal. Calcd (found) for $C_{19}H_{12}N_2Cl_4O_5U$: C, 31.34 (30.82); H, 1.66 (1.71); N, 3.85 (3.33). IR (KBr pellet): 3446, 2878, 2576, 1629, 1562, 1454, 1367, 1311, 1101, 917, 891, 814, 753, 604, 507 cm^{-1}.

Fabrication of the Bluish-Green OLED. The first step of the fabrication process was the cleaning of the ITO substrate with a detergent, acetone, isopropanol, ethanol, and deionized water successively for 10 min each in an ultrasonic bath. PEDOT:PSS as a hole-injection layer was spin-coated on a clean ITO substrate at a thickness of 60 nm and baked in an oven for 30 min at 120 °C. Following this step, a PVK:TPD:PBD:complex with a mass ratio of 100:10:40:5 (3.22 mg:0.32 mg:1.29 mg:0.16 mg) as a light-emitting layer was spin-coated on PEDOT:PSS at a thickness of 65 nm and baked in an oven for 30 min at 110 °C. Eventually, a thin layer of Ca/Al at a deposition rate of 2−3 Å at 8×10^{-8} mbar was placed on top of the organic film by thermal evaporation to fabricate devices with an emission area of 2 mm × 2 mm. All measurements were performed without encapsulation in air at ambient temperature.

Fabrication of the White OLED. The cleaning of the ITO substrate, preparation of the hole-injection layer, and baking were similar to the fabrication of the blue OLED. Following cleaning, hole-injection layering, and baking, a PVK:TPD:PBD:DCM:complex with a mass ratio of 100:10:40:5:0.25 (3.22 mg:0.32 mg:1.29 mg:0.16 mg:0.008 mg) as a light-emitting layer was spin-coated on PEDOT:PSS at a thickness of 65 nm and baked in an oven for 30 min at 110 °C. Similar to the fabrication of the bluish OLED, a thin layer of Ca/Al at a deposition rate of 2−3 Å at 8×10^{-8} mbar was placed on top of the organic film by thermal evaporation to fabricate devices with an emission area of 2 mm × 2 mm.

RESULTS AND DISCUSSION

Synthesis and Characterization. The reaction of 8-hydroxyquinoline and 5,7-dichloro-8-hydroxyquinoline with uranium acetate dihydrate in a solvothermal chamber in methanol resulted in the formation of $UO_2(C_9H_6NO)_2(CH_3OH)$ (**1**) and $UO_2(C_9H_4NOCl_2)_2(CH_3OH)$ (**2**), respectively. Notably, altering the 8-hydroxyquinoline derivative did not affect the structure of the complexes (Scheme 1). The prepared complexes were characterized by FTIR, UV−vis spectroscopy, and elemental analysis.

Scheme 1. Structural Drawings of the Prepared Complexes

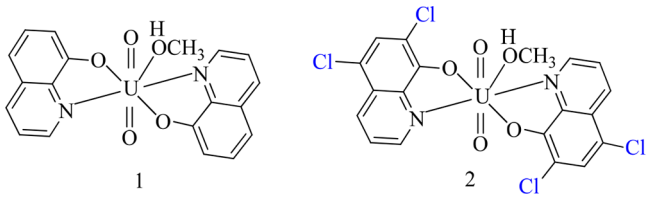

In the infrared spectra, the symmetric and asymmetric stretching vibration bands of U−O were in the range of 800−900 cm^{-1}.[50,51] Specifically, the stretching vibration bands of U−O in complexes **1** and **2** appeared at 830 and 901 cm^{-1} and at 891 and 917 cm^{-1}, respectively. The distinct broad -OH group stretching vibration band of 8-hydroxyquinoline and 3,5-dichloro-8-hydroxyquinoline in the range of 3000−3200 cm^{-1} was absent after reaction with uranium acetate and unambiguously showed deprotonation and coordination of the oxy group to uranium. The band around 1100 cm^{-1}, which was observed in the FTIR spectra of both complexes, was assigned to the stretching vibration of C−O of the C−O−M bond. The bands at around 1300 and 1400 cm^{-1} in the spectra were associated with the stretching vibrations of the C═C and C═N bonds in the 8-hydroxyquinoline components of the complexes.[50−52] The infrared spectra of complexes are shown in Figure S1.

Crystal Structures of $UO_2(C_9H_6NO)_2(CH_3OH)$ (1) and $UO_2(C_9H_4NOCl_2)_2(CH_3OH)$ (2). Complexes **1** and **2** crystallized in monoclinic space group $P2_1/n$. The asymmetric units consisted of complete metal−ligand complex molecules, which included one uranyl unit, one coordinated methanol, and two 8-oxyquinolinate or 5,7-dichloro-8-oxyquinolinate ligands. The latter were coordinated to uranium through the N and O atoms, giving five-membered metallacycles. The structure is best described as a pentagonal bipyramid with methanol as the fifth equatorial ligand (Figure 1). The oxido O atoms of the

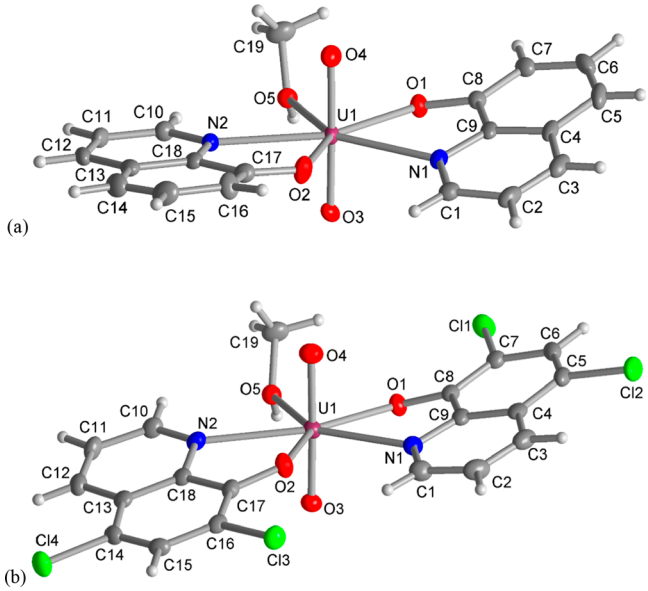

Figure 1. Molecular structures of complexes (a) **1** and (b) **2** (50% thermal ellipsoids).

quinolate ligands were located at a *trans* position to each other. The uranyl oxido ligands have an approximately linear orientation at an angle of 176.30(16)° in **1** and 176.42(8)° in **2**. The U═O bond lengths are between 1.76 and 1.79 Å. The crystallography data and selected bond lengths are listed in Tables S1−S3.

Thermal Properties. During TGA (Figure S2), the first mass loss of 5.5% at around 210 °C of complex **1** was associated with the release of coordinated methanol. This mass loss was in excellent agreement with the calculated value of 5.42%. The second mass loss of 47% between ∼370 and ∼650 °C was due to the decomposition and combustion of the quinolate ligands. The result was in fair agreement with the calculated value of 49%. The thermal behavior of complex **2** was similar to that of complex **1**. However, the coordinated methanol of complex **2** was released at around 220 °C with a mass loss of ∼4%. This temperature was somewhat higher than that in complex **1**. The release of coordinated methanol at the higher temperature in complex **2** probably was due to the presence of two electronegative substituents on the 8-oxyquinolinate ligands. The second mass loss of 42% between 390 and 650 °C in the thermogram of complex **2** (similar to that of complex **1**) was also associated with the decomposition and combustion of the ligands in the complex. This mass loss

https://dx.doi.org/10.1021/acs.inorgchem.0c02242
Inorg. Chem. 2020, 59, 17028−17037

was close to the calculated value of 41%. On the basis of the results of thermal analysis of complexes, we concluded that the prepared complexes were stable up to 210−220 °C, which makes them suitable for the fabrication of devices using high-temperature processing techniques.

Theoretical Calculations. Density functional theory (DFT) at the PBE0/Def-TZVP&SARC-ZORA-TZVP level of theory was carried out to obtain the orbital energies of $UO_2(C_9H_6NO)_2(CH_3OH)$ (**1**) and $UO_2(C_9H_4NOCl_2)_2(CH_3OH)$ (**2**). On the basis of the calculations for complex **1**, the highest occupied molecular orbital (HOMO) is located on the p orbitals of the uranyl oxido oxygen atoms and one of the 8-oxyquinolinate ligands. The corresponding contributions are ∼14.6% and ∼85.4%, respectively. It was also found that the corresponding lowest unoccupied molecular orbital (LUMO) is located on the f orbitals of uranium and the p orbitals of 8-oxyquinolinate, which have 11.5% and 88.5% contributions, respectively. Similar data were found for complex **2**; the HOMO is located on the p orbitals of uranyl oxygen and one of the 5,7-dichloro-8-hydroxyquinoline ligands. The oxygen and 5,7-dichloro-8-oxyquinolinate contributions are ∼7.5% and ∼92.5%, respectively. The LUMO for complex **2** is located on the f orbitals of uranium and the p orbital of the 8-hydroxyquinoline ligand, and they contribute ∼24.5% and ∼75.5%, respectively. As is obvious from the data, the HOMO in both complexes is located entirely on ligands and mainly on quinolinate ligands. On the contrary, the LUMO is situated mainly on quinolinate ligands and, to some extent, on the uranium metal atom. Therefore, these complexes are ideal substrates for ligand-to-metal charge-transfer (LMCT) transitions and specifically for intraligand charge-transfer (ILCT) transitions. The HOMO and LUMO orbitals and the bandgap energy are shown in Figure 2 and Table 1.

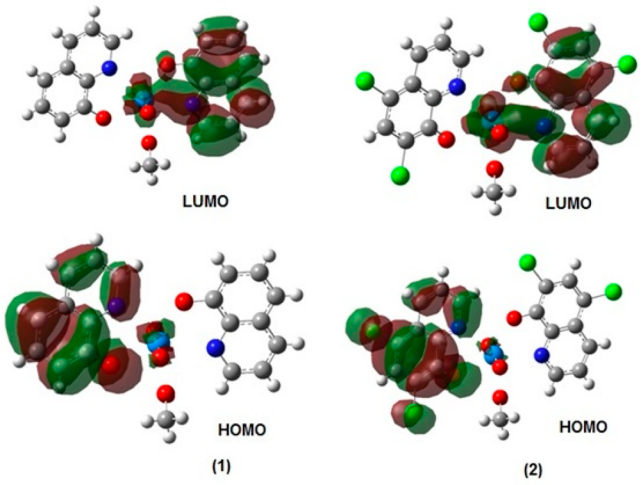

Figure 2. HOMO and LUMO orbitals of complexes **1** and **2**.

Table 1. HOMO and LUMO Energies and Bandgaps of Complexes 1 and 2

	HOMO (eV)	LUMO (eV)	bandgap (eV)
1	−5.46	−2.21	3.26
2	−5.60	−2.58	3.02

The DFT calculations for both complexes indicate that the large orbital molecular coefficients in both the HOMO and the LUMO are located on uranyl and one of the quinoline ligands. The results also revealed that the bandgap is 3.26 eV for complex **1**, while that for complex **2** decreases to 3.02 eV, suggesting bluish-green emission.[53,54] This decrease may be a consequence of the chlorine electron-withdrawing effect, which in turn increases the fluorescence intensity of this complex. The decrease in energy levels in the presence of chlorine verifies that the ILCT transitions of 8-oxyquinolinate ligands are critical in the absorption and fluorescence spectra of these complexes.[55] Furthermore, to confirm this level of theory and their alignment with the experiment absorption, the theoretical absorption spectra by time-dependent density functional theory (TD-DFT)[56] were recorded for the low-lying excited states (>300 nm). As one can see in Figure S3, the theoretical absorption spectra exhibited the same trend as the experiment and confirmed the trend of the decreasing HOMO/LUMO gap from **1** to **2**.

UV−Vis Absorption Spectra. The UV−vis spectra of the uranium complexes and the free 8-hydroxyquinoline and 5,7-dichloro-8-hydroxyquinoline ligands were measured to obtain their photoresponsive regions. The absorption spectra of 8-hydroxyquinoline and 5,7-chloro-8-hydroxyquinoline, as shown in Figure S4, exhibited absorption at 225−375 nm.[7,57] The electronic absorption spectra of the complexes were studied in THF. The results are illustrated in Figure 3.

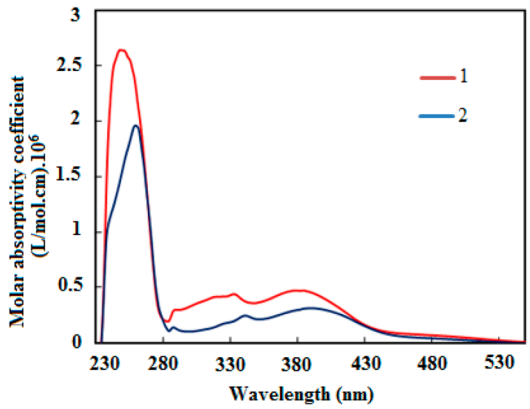

Figure 3. UV−vis spectra of $UO_2(C_9H_6NO)_2(CH_3OH)$ (**1**) and $UO_2(C_9H_4NOCl_2)_2(CH_3OH)$ (**2**) in THF (1.0×10^{-6} mol L^{-1}).

Complexes **1** and **2** showed three absorptions at 252, 334, and 383 nm and 261, 342, and 393 nm, respectively. The electronic transitions of $UO_2(C_9H_4NOCl_2)_2(CH_3OH)$ (**2**) emerged at higher wavelengths compared with those of $UO_2(C_9H_6NO)_2(CH_3OH)$ (**1**), which is due to the chlorine-withdrawing effect and stabilization of the π^* state. These data are in accordance with DFT studies.

Photoluminescence Studies. The photoluminescence spectra of the complexes were recorded in solution and solid state at ambient temperature under excitation at 350 nm (Figure 4a,b). Both complexes showed similar photoluminescence spectra, but their intensities and positions were influenced by the electron-withdrawing groups.[58] The equation reported by Parker and Rees (eq 1) was employed to estimate the quantum yields of complexes **1** and **2**.[59,60]

$$\frac{F_2}{F_1} = \frac{\varphi_2 \varepsilon_2 d_2 c_2}{\varphi_1 \varepsilon_1 d_1 c_1} \quad (1)$$

https://dx.doi.org/10.1021/acs.inorgchem.0c02242
Inorg. Chem. 2020, 59, 17028−17037

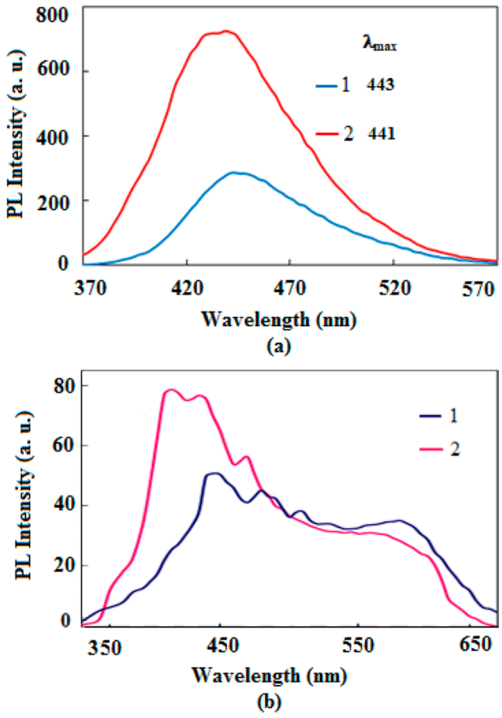

Figure 4. Photoluminescence spectra of complexes in (a) solution (THF, 1.0×10^{-6} mol L^{-1}) and (b) the solid state, at an excitation wavelength of 350 nm at 273 K.

where F is the fluorescence area, φ is the relative quantum yield, c and ε are the sample's concentration and extinction coefficient, respectively, and d is the solution thickness. Relative PL quantum yield values of 0.68 and 0.72 were attained for complexes **1** and **2**, respectively.

The fluorescence quantum yield increased from **1** to **2**. A decline in energy levels was observed by increasing the electron affinity or electron-withdrawing effect of the aromatic ring; consequently, the fluorescence quantum yield increased.[55] It is worth noting that, because the metal-centered PL emission of the uranyl ion is expected as a broad band in the range of 480–570 nm with a λ_{max} of 508 nm,[61,62] the dominant ligand emissions obscured the PL emissions of complexes. For verification, the PL spectra of 8-hydroxyquinoline, 5,7-dichloro-8-hydroxyquinoline (Figure S5), and the final complexes were recorded in THF at ambient temperature with an excitation wavelength of 350 nm. This result confirmed that the emission of the ligand obscured the metal-centered emission band. Apparently, ligand-centered (LC) transitions in the conjugated system facilitated the emission.

Bluish-Green and White Organic Light-Emitting Devices. Compound **1**, with no electron-withdrawing groups, and compound **2**, with electron-withdrawing groups, were used to confirm the influence of the electron-withdrawing groups on the fluorescence in the OLED structure. The complexes functioned as effective blue fluorescent materials in which the HOMO, LUMO, and bandgap energy in complex $UO_2(C_9H_6NO)_2(CH_3OH)$ (**1**) were −5.46, −2.21, and 3.26 eV, respectively. In complex $UO_2(C_9H_4NOCl_2)_2(CH_3OH)$ (**2**), these values were −5.60, −2.58, and 3.02 eV, respectively. Next, BCP was used as a hole blocker, and it was coated on a PVK:TPD:PBD complex using the vapor-deposition method at 1 A/s at a thickness of 8 nm. Ca was then coated on BCP by vapor deposition at a thickness of 20 nm. The final layer, which was aluminum, was coated on Ca at a thickness of 120 nm. The active area of the prepared devices was 3 mm × 1.5 mm. The fundamental structures of the OLEDs were glass/ITO/PEDOT:PSS (60 nm)/PVK:TPD:PBD:complex (65 nm)/BCP (8 nm)/Ca (20 nm)/Al (120 nm). The addition of DCM to the active layer resulted in a white light-emitting diode. It was observed that if the proportion was adjusted to 100:10:40:5:0.125, the fabricated OLED functioned as a bluish-white light-emitting device. In the latter case, the fundamental structures of the OLED were glass/ITO/PEDOT:PSS (60 nm)/PVK:TPD:PBD:complex:DCM (65 nm)/BCP (8 nm)/Ca (20 nm)/Al (120 nm). Furthermore, a 0.5:5 proportion of the DCM:complex could be used in the fabrication of a yellow OLED. The structures of the compounds that were used to fabricate the OLEDs are shown in Scheme S1, and the structures of the blue and white OLEDs are illustrated in Figures 5 and 6, respectively.[63−66]

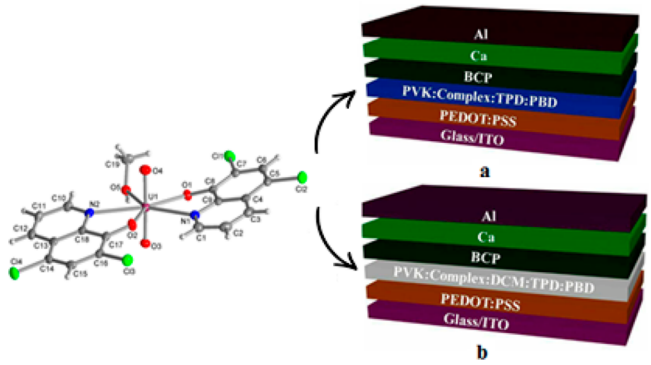

Figure 5. Device structures of (a) the bluish-green OLED and (b) the white OLED.

Electroluminescence Studies. The electroluminescence spectra of the fabricated devices were investigated at 14 V. The results are shown in Figure 7. The chlorine-containing complex had a higher emission intensity and quantum yield compared with those of the hydrogen-containing complex; thus, it showed superior performance.

The current−voltage characteristics of the prepared OLEDs are shown in Figure 8. When a bias voltage was applied, electrons and holes were injected into the active layer, and the current density increased. Notably, complex $UO_2(C_9H_6NO)_2(CH_3OH)$ (**1**) required a driving voltage higher than that of the other complex because of its higher LUMO level and thus its energy barrier. The increase in the energy barrier prevented an effective transfer of charge into the dye molecules, therefore increasing the turn-on voltage. The highest current density was ascribed to the white OLED because of its efficient transfer of charge into the fluorescent molecules. It was observed that the net device current density of the complex containing the 5,7-dichloro-8-hydroxyquinoline ligand was higher than that of the complex containing 8-hydroxyquinoline, which was correlated to its molecular energy levels. The $UO_2(C_9H_4NOCl_2)_2(CH_3OH)$ (**2**) complex possessed a LUMO level much lower than that of $UO_2(C_9H_6NO)_2(CH_3OH)$ (**1**) with the PBD energy level, leading to the ease of electron transfer, exciton formation, and light emission. Therefore, complex **2** was used to fabricate high-performance white OLEDs.

Figure 9 presents a schematic energy diagram of the white light-emitting diodes. In the beginning, electrons from

https://dx.doi.org/10.1021/acs.inorgchem.0c02242
Inorg. Chem. 2020, 59, 17028−17037

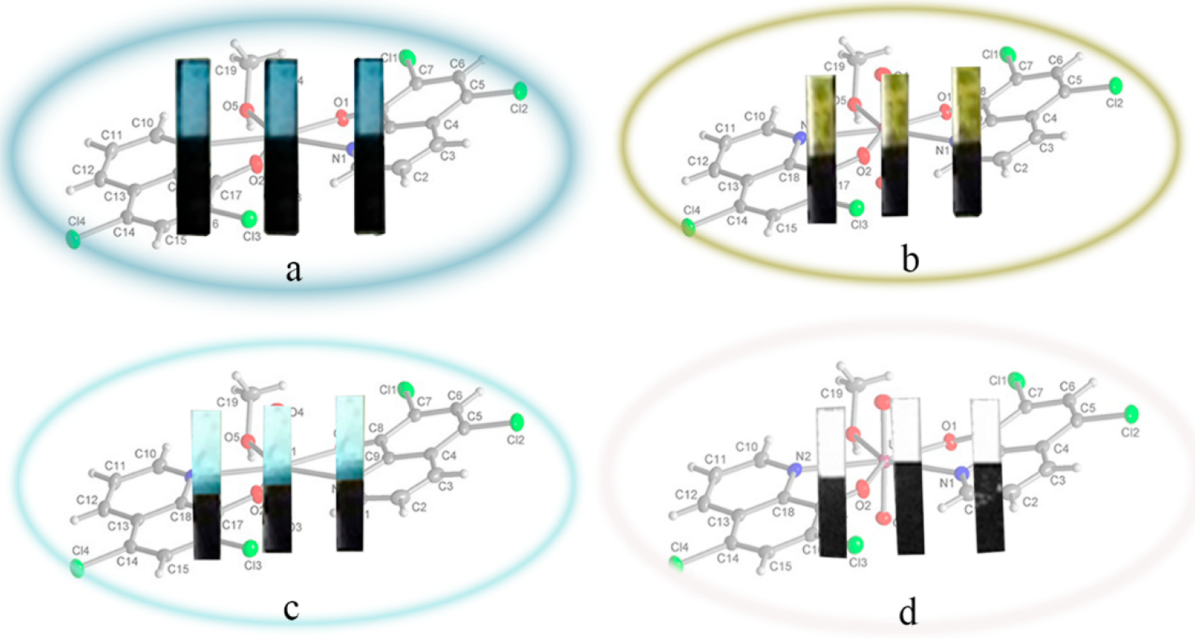

Figure 6. (a) Bluish-green (DCM:complex, 0:5), (b) yellow (DCM:complex, 0.5:5), (c) bluish-white (DCM:complex, 0.125:5), and (d) white (DCM:complex, 0.25:5) OLEDs [DCM = 4-(dicyanomethylene)-2-methyl-6-(4-dimethylaminostyryl)-4*H*-pyran (Scheme S1)].

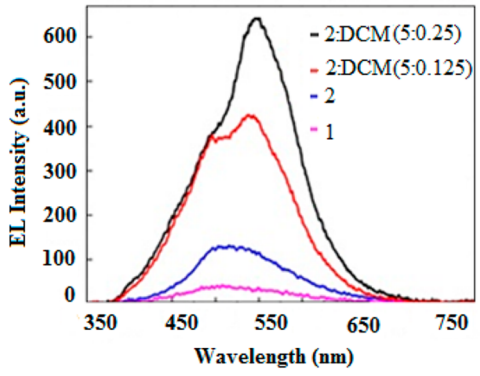

Figure 7. Electroluminescence spectra of the prepared devices at 14 eV.

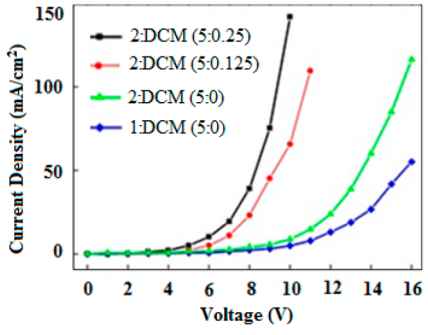

Figure 8. *J*−*V* curves of the fabricated OLEDs at various fluorescence:dye ratios.

aluminum and calcium are injected into the LUMO level of BCP as the hole blocker layer and PBD as the electron transport layer. Then, the electrons from PBD are transported to **2**:DCM as a light-emitting layer. Next, holes from ITO are injected into the HOMO level of PEDOT:PSS as a hole

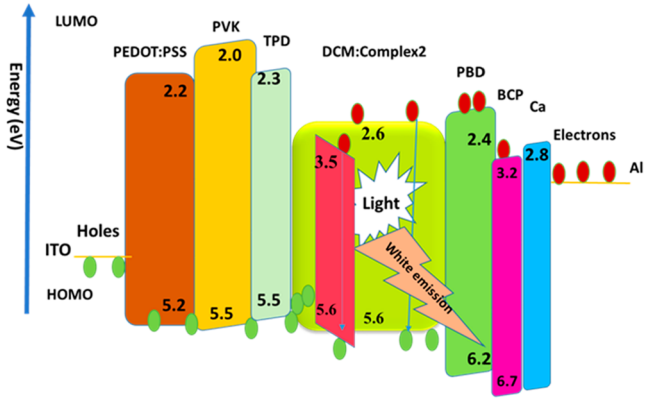

Figure 9. HOMO and LUMO energy levels of the uranium complex and materials used to fabricate white OLEDs.

injector layer, and subsequently to PVK and TPD as the hole transport layer. Finally, holes move to **2**:DCM as the light-emitting layer; eventually, the recombination of the electron−hole occurs, and a white electroluminescence band appears. Because there is coulombic interaction between holes in the HOMO level and electrons in LUMO levels, this results in the generation of excitons in this layer. The demolition of excitons emits photons that have the same energy as the bandgap or higher than it. Therefore, for the transfer of excitons to HOMO and LUMO levels, an energy transfer between the host material and emissive dopants must exist. As one can derive from Figure 9, HOMO and LUMO levels of DCM with values of −3.5 and −5.6 eV, respectively, lie between the HOMO and LUMO levels of the uranium complex used to fabricate the OLED (Table 1). This caused electrons and holes to accumulate at DCM molecules and achieve electron/hole recombination. Two recombinations occurred, including radiative recombination and trap recombination. The former recombination leads to the observation of electroluminescence

https://dx.doi.org/10.1021/acs.inorgchem.0c02242
Inorg. Chem. 2020, 59, 17028−17037

from DCM, but later recombination in contrast to the former did not result in electroluminescence under this condition. It should be mentioned that trap levels can shorten the device lifetime due to the thermal aging and impurity diffusion at various applied voltages. Figure 10 shows the luminescence−

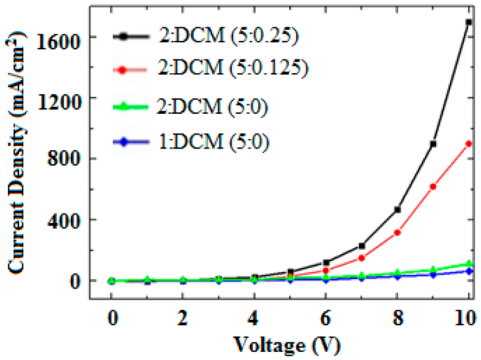

Figure 10. Luminance−voltage characteristics of the fabricated devices.

voltage characteristics of the fabricated devices. The maximum luminescence was assigned to the white OLED. The luminescence intensity changed as follows: **2**:DCM (5:0.25) > **2**:DCM (5:0.125) > **2** > **1**. This trend indicated that the performance of the OLEDs was causally related to the chemical structures of the moieties. The 5,7-dichloro-8-hydroxyquinoline ligand was employed to prepare complex **2** and subsequently to fabricate the OLEDs, which provided a superior fluorescence compared to that prepared without chlorine. The external quantum efficiency (EQE) was obtained from luminance, current density, and EL spectral data. Maximum quantum efficiencies of 12.34% and 10.12% were achieved for the white device with dopants ratio of 5:0.25 and 5:0.125 (**2**:DCM), respectively (Table 2). The more balanced hole and electron injections in the device are the prime reason for the higher efficiency and improvement of the device with a dopant concentration of 5:0.25 (**2**:DCM) with respect to other devices.

Table 2. Device Characteristics of Bluish and White OLEDs Based on the Uranium Complexes[a]

	1	**2**	**2**:DCM (5:0.125)	**2**:DCM (5:0.25)
peak emission (nm)	500	500	494, 540	490, 550
CIE (*x*, *y*)	(0.26, 0.43)	(0.28, 0.45)	(0.29, 0.43)	(0.30, 0.42)
fwhm (nm)	140	130	130	120
CRI			56	55
CCT			6801	6456
turn-on voltage (V)	10	9	6	5
current density (mA cm^{-1}), at 10 V	4.8	8.7	65.7	141.9
luminance (cd m^{-2}), at 10 V	60	110	900	1700
current efficiency (cd A^{-1})	1.25	1.26	1.37	1.20
power efficiency (lm W^{-1})	0.39	0.44	0.72	0.75
maximum EQE (%)	7.02	8.23	10.12	12.34

[a]Abbreviations: CRI, color rending index; EQE, external quantum efficiency.

Figure 11 presents a chromaticity diagram of the fabricated devices. The electroluminescence spectral data were used in

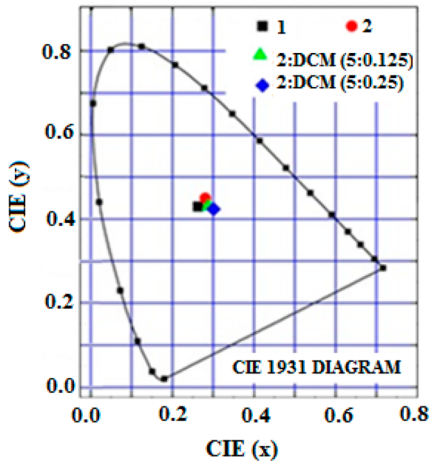

Figure 11. Variations in the CIE 1931 chromaticity coordinates of the prepared OLEDs.

the MATLAB software to derive at the CIE coordinates. Obviously, the emission obtained from the **2**:DCM (5:0.25) and **2**:DCM (5:0.125) layer overlaps between the emission of uranium complexes at around 500 nm and the emission of DCM at 580 nm. This can be elucidated by considering the exciton diffusion length of ∼8 nm in organic thin films.[67,68] Because in **2**:DCM (5:0.125) the number of DCM molecules is lower in the uranium complex, excitons formed at uranium molecules have to diffuse before energy is transferred to DCM. Therefore, they can recombine on uranium molecules and contribute to the uranium spectral signature. However, with an increase in the ratio to 5:0.25 (**2**:DCM), the number of DCM molecules in the uranium complex increased, and concomitantly, the energy-transfer radius decreased. Consequently, the emission of the uranium complex in the EL spectrum decreased, and recombination of excitons at DCM molecules materialized. In addition, as Figure 7 shows, with an increase in the amount of DCM molecules, the full width at half-maximum (fwhm) changed, which has a direct relationship with CIE coordinates. The Commission International de 1'Eclairage (CIE) coordinates of the devices containing complex **1** and complex **2** were far from cx = 0.33 and cy = 0.33, which are the ideal white point coordinates. When the DCM dye molecule was incorporated into the active layer, the chromaticity coordinates moved toward the white point, and with an increase in its concentration, the CIE coordinates were made to approach the reference white coordinates. The characterizations of the prepared devices are listed in Table 2. According to the results, the chlorine-containing sample possessed a lower turn-on voltage and a higher current density. However, the difference in current efficiency was negligible. It is well-known that the equal-energy white correlated color temperature (CCT) was 6456, which can be approached by introducing the appropriate concentration of an orange dye molecule. Figure 11 shows that the complex's optical properties, such as emission color, were directly associated with the ligand and thus could be controlled by the careful engineering of the chemical structure. As observed in the EL spectra and confirmed by the CIE chromaticity diagram, the synthesized uranium complexes provided a broad emission

https://dx.doi.org/10.1021/acs.inorgchem.0c02242
Inorg. Chem. 2020, 59, 17028−17037

spectrum, which could be used to fabricate high-quality white light sources.[57,69,70]

CONCLUSIONS

In this study, two uranium complexes were synthesized through solvothermal and ultrasonic methods using 8-hydroxyquinoline and 5,7-dichloro-8-hydroxyquinoline ligands. The prepared complexes were characterized by various techniques and utilized as a fluorescent dye in the fabrication of white and blue OLEDs. The photophysical investigation of the prepared complexes and fabricated OLEDs showed that their optical properties strongly corresponded with the properties of the ligands that were employed to synthesize the complexes. Therefore, by the complexation of appropriate ligands with actinide-series elements, it is possible to prepare coordination complexes, tune their optical properties, and subsequently fabricate highly efficient light sources.

ASSOCIATED CONTENT

Supporting Information

The Supporting Information is available free of charge at https://pubs.acs.org/doi/10.1021/acs.inorgchem.0c02242.

Crystal data and refinements of complexes (Table S1), selected bond lengths and angles of complexes (Tables S2 and S3), IR spectra of complexes (Figure S1), thermogram of complexes (Figure S2), theoretical absorption spectra of complexes (Figure S3), UV spectra of ligands (Figure S4), PL spectra of ligands (Figure S5), and structures of materials used to fabricate OLEDs (Scheme S1) (PDF)

Accession Codes

CCDC 1585374−1585375 contain the supplementary crystallographic data for this paper. These data can be obtained free of charge via www.ccdc.cam.ac.uk/data_request/cif, or by emailing data_request@ccdc.cam.ac.uk, or by contacting The Cambridge Crystallographic Data Centre, 12 Union Road, Cambridge CB2 1EZ, UK; fax: +44 1223 336033.

AUTHOR INFORMATION

Corresponding Authors

Mostafa M. Amini − *Department of Chemistry, Shahid Beheshti University, Tehran 1983963113, Iran;* orcid.org/0000-0003-2974-1024; Email: m-pouramini@sbu.ac.ir

Christoph Janiak − *Institut für Anorganische Chemie und Strukturchemie Heinrich-Heine Universität, D-40204 Düsseldorf, Germany;* orcid.org/0000-0002-6288-9605; Email: janiak@uni-duesseldorf.de

Authors

Khodabakhsh Darzinezhad − *Department of Chemistry, Shahid Beheshti University, Tehran 1983963113, Iran*

Mohammad Janghouri − *Faculty of Industrial Technologies, Urmia University of Technology, Urmia 5716693187, Iran*

Ezeddin Mohajerani − *Laser and Plasma Research Institute, Shahid Beheshti University, Tehran 1983963113, Iran*

Mohammad-Reza Fathollahi − *Laser and Plasma Research Institute, Shahid Beheshti University, Tehran 1983963113, Iran*

Zahra Jamshidi − *Chemistry Department, Sharif University of Technology, Tehran 11155-9516, Iran;* orcid.org/0000-0003-0976-1132

Complete contact information is available at: https://pubs.acs.org/10.1021/acs.inorgchem.0c02242

Notes

The authors declare no competing financial interest.

ACKNOWLEDGMENTS

The authors gratefully acknowledge the financial support (Grant S600/43) from the Research Council of Shahid Beheshti University. The work of C.J. is funded by the Deutsche Forschungsgemeinschaft (DFG, German Research Foundation), Project 396890929/GRK 2482.

REFERENCES

(1) Natrajan, L. S. Developments in the photophysics and photochemistry of actinide ions and their coordination compounds. *Coord. Chem. Rev.* **2012**, *256*, 1583−1603.

(2) Tsushima, S.; Götz, C.; Fahmy, K. Photoluminescence of uranium(VI): Quenching mechanism and role of uranium(V). *Chem. - Eur. J.* **2010**, *16*, 8029−8033.

(3) Liang, L. L.; Zhang, R. L.; Weng, N. S.; Zhao, J. S.; Liu, C. Y. Synthesis, structures, and photoluminescent properties of two uranium complexes constructed by a flexible zwitterion ligand. *Inorg. Chem. Commun.* **2016**, *64*, 56−58.

(4) Thangavelu, S. G.; Butcher, R. J.; Cahill, C. L. Role of N-Donor sterics on the coordination environment and dimensionality of uranyl thiophenedicarboxylate coordination polymers. *Cryst. Growth Des.* **2015**, *15*, 3481−3492.

(5) Geipel, G. Some aspects of actinide speciation by laser-induced spectroscopy. *Coord. Chem. Rev.* **2006**, *250*, 844−854.

(6) Mihalcea, I.; Henry, N.; Loiseau, T. Revisiting the uranyl-phthalate system: Isolation and crystal structures of two types of uranyl-organic frameworks (UOF). *Cryst. Growth Des.* **2011**, *11*, 1940−1947.

(7) Jiang, Y. S.; Yu, Z. T.; Liao, Z. L.; Li, G. H.; Chen, J. S. Syntheses and photoluminescent properties of two uranyl-containing compounds with extended structures. *Polyhedron* **2006**, *25*, 1359−1366.

(8) Borkowski, L. A.; Cahill, C. L. Crystal engineering with the uranyl cation II. Mixed aliphatic carboxylate/aromatic pyridyl coordination polymers: synthesis, crystal structures, and sensitized luminescence. *Cryst. Growth Des.* **2006**, *6*, 2248−2259.

(9) Frisch, M.; Cahill, C. L. Synthesis, structure and fluorescent studies of novel uranium coordination polymers in the pyridinedicarboxylic acid system. *Dalton Trans.* **2006**, 4679−4690.

(10) Zheng, Y.-Z.; Tong, M.-L.; Chen, X.-M. Synthesis, structure and photoluminescent studies of two novel layered uranium coordination polymers constructed from UO(OH) polyhedra and pyridinedicarboxylates. *Eur. J. Inorg. Chem.* **2005**, *2005*, 4109−4117.

(11) Pan, Q.-J.; Shamov, G. A.; Schreckenbach, G. Binuclear uranium(VI) complexes with a "pacman" Expanded porphyrin: Computational evidence for highly unusual bis-actinyl structures. *Chem. - Eur. J.* **2010**, *16*, 2282−2290.

(12) Mei, L.; Wang, L.; Yuan, L. Y.; An, S. W.; Zhao, Y. L.; Chai, Z. F.; Burns, P. C.; Shi, W. Q. Supramolecular inclusion-based molecular integral rigidity: a feasible strategy for controlling the structural connectivity of uranyl polyrotaxane networks. *Chem. Commun.* **2015**, *51*, 11990−11993.

(13) Andrews, M. B.; Cahill, C. L. Uranyl bearing hybrid materials: Synthesis, speciation, and solid- state structures. *Chem. Rev.* **2013**, *113*, 1121−1136.

(14) Thangavelu, S. G.; Cahill, C. L. A family of uranyl coordination polymers containing O-Donor dicarboxylates and trispyridyltriazine guests. *Cryst. Growth Des.* **2016**, *16*, 42−50.

(15) Qiu, J.; Vlaisavljevich, B.; Jouffret, L.; Nguyen, K.; Szymanowski, J. E. S.; Gagliardi, L.; Burns, P. C. Cation templating and electronic structure effects in uranyl cage clusters probed by the

isolation of peroxide-bridged uranyl dimers. *Inorg. Chem.* **2015**, *54*, 4445−4455.
(16) Mei, L.; Wang, C.-Z.; Zhu, L.-Z.; Gao, Z.-Q.; Chai, Z.-F.; Gibson, J. K.; Shi, W.-Q. Exploring new assembly modes of uranyl terephthalate: Templated syntheses and structural regulation of a series of rare 2D → 3D polycatenated frameworks. *Inorg. Chem.* **2017**, *56*, 7694−7706.
(17) Mei, L.; Wu, Q.-Y.; Liu, C.-M.; Zhao, Y.-L.; Chai, Z.-F.; Shi, W.-Q. Exploring new assembly modes of uranyl terephthalate: Templated syntheses and structural regulation of a series of rare 2D → 3D polycatenated frameworks. *Chem. Commun.* **2014**, *50*, 3612−3615.
(18) Thuery, P. Sulfonate complexes of actinide ions: Structural diversity in uranyl complexes with 2-sulfobenzoate. *Inorg. Chem.* **2013**, *52*, 435−447.
(19) Zheng, T.; Wu, Q. Y.; Gao, Y.; Gui, D. X.; Qiu, S. W.; Chen, L. H.; Sheng, D. P.; Diwu, J.; Shi, W. Q.; Chai, Z. F.; Albrecht-Schmitt, T. E.; Wang, S. A. Probing the influence of phosphonate bonding modes to uranium(VI) on structural topology and stability: A complementary experimental and computational investigation. *Inorg. Chem.* **2015**, *54*, 3864−3874.
(20) An, S. W.; Mei, L.; Wang, C. Z.; Xia, C. Q.; Chai, Z. F.; Shi, W. Q. The first case of actinide triple helices: pH dependent structural evolution and kinetics controlled transformation of two supramolecular conformational isomers. *Chem. Commun.* **2015**, *51*, 8978−8981.
(21) Parker, T. G.; Cross, J. N.; Polinski, M. J.; Lin, J.; Albrecht-Schmitt, T. E. Ionothermal and hydrothermal flux syntheses of five new uranyl phosphonates. *Cryst. Growth Des.* **2014**, *14*, 228−235.
(22) Liu, W.; Dai, X.; Xie, J.; Silver, M. A.; Zhang, D.; Wang, Y.; Cai, Y.; Diwu, J.; Wang, J.; Zhou, R.; Chai, Z.; Wang, S. Preparation, structures, and photocatalytic properties of three new uranyl-organic assembly compounds. *ACS Appl. Mater. Interfaces* **2018**, *10*, 4844−4850.
(23) Xie, J.; Wang, Y.; Silver, M. A.; Liu, W.; Duan, T.; Yin, X.; Chen, L.; Diwu, J.; Chai, Z.; Wang, S. Tunable 4f/5f bimodal emission in europium-incorporated uranyl coordination polymers. *Inorg. Chem.* **2018**, *57*, 575−582.
(24) Li, P.; Vermeulen, N. A.; Malliakas, C. D.; Gómez-Gualdrón, D. A.; Howarth, A. J.; Mehdi, B. L.; Dohnalkova, A.; Browning, N. D.; O'Keeffe, M.; Farha, O. K. Bottom-up construction of a superstructure in a porous uranium-organic crystal. *Science* **2017**, *356*, 624−627.
(25) Li, P.; Vermeulen, N. A.; Gong, X.; Malliakas, C. D.; Stoddart, J. F.; Hupp, J. T.; Farha, O. K. Design and synthesis of a water-stable anionic uranium-based metal−organic framework (MOF) with ultra large pores. *Angew. Chem., Int. Ed.* **2016**, *55*, 10358−10362.
(26) Xie, J.; Wang, Y.; Liu, W.; Yin, X.; Chen, L.; Zou, Y.; Diwu, J.; Chai, Z.; Albrecht-Schmitt, T. E.; Liu, G.; Wang, S. Highly sensitive detection of ionizing radiations by a photoluminescent uranyl organic framework. *Angew. Chem., Int. Ed.* **2017**, *56*, 7500−7504.
(27) Wang, Y.; Liu, Z.; Li, Y.; Bai, Z.; Liu, W.; Wang, Y.; Xu, X.; Xiao, C.; Sheng, D.; Diwu, J.; Su, J.; Chai, Z.; Albrecht-Schmitt, T. E.; Wang, S. Umbellate distortions of the uranyl coordination environment result in a stable and porous polycatenated framework that can effectively remove cesium from aqueous solutions. *J. Am. Chem. Soc.* **2015**, *137*, 6144−6147.
(28) Wang, X.; Wang, Y.; Dai, X.; Silver, M. A.; Liu, W.; Li, Y.; Bai, Z.; Gui, D.; Chen, L.; Diwu, J.; Zhou, R.; Chai, Z.; Wang, S. Phase transition triggered aggregation-induced emission in a photoluminescent uranyl-organic framework. *Chem. Commun.* **2018**, *54*, 627−630.
(29) Wang, Y.; Yin, X.; Liu, W.; Xie, J.; Chen, J.; Silver, M. A.; Sheng, D.; Chen, L.; Diwu, J.; Liu, N.; Chai, Z.; Albrecht-Schmitt, T. E.; Wang, S. Emergence of uranium as a distinct metal center for building intrinsic X-ray scintillators. *Angew. Chem., Int. Ed.* **2018**, *57*, 7883−7887.
(30) Liu, W.; Xie, J.; Zhang, L.; Silver, M. A.; Wang, S. A hydrolytically stable uranyl organic framework for highly sensitive and selective detection of Fe^{3+} in aqueous media. *Dalton Trans.* **2018**, *47*, 649−653.
(31) Mirzaei, M.; Hassanpoor, A.; Bauza, A.; Mague, J. T.; Frontera, A. A new solvated complex of the uranyl ion (UO_2^{2+}) with 8-hydroxyquinoline. *Inorg. Chim. Acta* **2015**, *426*, 136−141.
(32) Amirthalingam, V. Crystallographic studies on sodium uranyl-8-quinolinate, $Na.UO_2.(C_9H_6NO)_3$. *Acta Crystallogr.* **1960**, *13*, 61.
(33) Horton, G. R.; Wendlandt, W. W. X-Ray and differential thermal analysis studies on the 8-quinolinol and substituted 8-quinolinol metal chelates of thorium(IV), uranium(VI) and scandium(III). *J. Inorg. Nucl. Chem.* **1963**, *25*, 247−252.
(34) Hall, D.; Rae, A. D.; Waters, T. N. The crystal structure of the chloroform solvate of dioxodi-8-quinolinolato-8-quinolinoluranium-(VI). *Acta Crystallogr.* **1967**, *22*, 258−268.
(35) Sasikumar, P.; Muthiah, P. T. Triaqua(l-7-iodo-8-oxidoquinoline-5-sulfonato κ^2N,O^8)dioxidouranium(VI) dehydrate. *Acta Crystallogr., Sect. C: Cryst. Struct. Commun.* **2010**, *C66*, m48−m50.
(36) Singh, D.; Nishal, V.; Bhagwan, S.; Saini, R. K.; Singh, I. Electroluminescent materials: Metal complexes of 8-hydroxyquinoline-A review. *Mater. Des.* **2018**, *156*, 215−228.
(37) Lee, J.-H.; Chen, C.-H.; Lee, P.-H.; Lin, H.-Y.; Leung, M.-K.; Chiu, T.-L.; Lin, C.-F. Blue organic light-emitting diodes: current status, challenges, and future outlook. *J. Mater. Chem. C* **2019**, *7*, 5874−5888.
(38) Darzinezhad, Kh.; Amini, M. M.; Mohajerani, E.; Armaghan, M.; Knedel, T. O.; Abareghi, A.; Janiak, C. Fabrication of blue organic light-emitting diodes from novel uranium complexes: synthesis, characterization, and electroluminescence studies of uranium anthracene-9-carboxylate complexes. *Dalton Trans.* **2019**, *48*, 3695−3703.
(39) Perrin, D. D.; Armarego, W. L. F.; Perrin, D. R. *Purification of laboratory chemicals*, 2nd ed.; Springer: New York, 1980.
(40) *SAINT*; D. R. Bruker Analytical X-ray Systems: Madison, WI, 1997−2006.
(41) Sheldrick, G. M. *Program SADABS: Area-detector absorption correction*; University of Göttingen: Göttingen, Germany, 1996.
(42) Sheldrick, G. M. A short history of *SHELX*. *Acta Crystallogr., Sect. A: Found. Crystallogr.* **2008**, *64*, 112−122.
(43) Brandenburg, K. *Diamond (version 3.2), crystal and molecular structure visualization, crystal impact*; K. Brandenburg & H. Putz Gbr: Bonn, Germany, 2009.
(44) Adamo, C.; Barone, V. Toward reliable density functional methods without adjustable parameters: The PBE0 model. *J. Chem. Phys.* **1999**, *110*, 6158−6170.
(45) Zhuang, J.; Abella, L.; Sergentu, D.-C.; Yao, Y.-R.; Jin, M.; Yang, W.; Zhang, X.; Li, X.; Zhang, D.; Zhao, Y.; Li, X.; Wang, S.; Echegoyen, L.; Autschbach, J.; Chen, N. Diuranium(IV) carbide cluster U2C2 stabilized inside fullerene cages. *J. Am. Chem. Soc.* **2019**, *141*, 20249−20260.
(46) Pantazis, D. A.; Neese, F. All-electron scalar relativistic basis sets for the actinides. *J. Chem. Theory Comput.* **2011**, *7*, 677−684.
(47) Lenthe, E. v.; Baerends, E. J.; Snijders, J. G. Relativistic regular two-component Hamiltonians. *J. Chem. Phys.* **1993**, *99*, 4597−4610.
(48) (a) Schäfer, A.; Horn, H.; Ahlrichs, R. Fully optimized contracted Gaussian basis sets for atoms Li to Kr. *J. Chem. Phys.* **1992**, *97*, 2571−2577. (b) Weigend, F.; Ahlrichs, R. Balanced basis sets of split valence, triple zeta valence and quadruple zeta valence quality for H to Rn: Design and assessment of accuracy. *Phys. Chem. Chem. Phys.* **2005**, *7*, 3297−3305.
(49) Neese, F. Wiley Interdiscip. *Wiley Interdiscip. Rev.: Comput. Mol. Sci.* **2012**, *2*, 73−78.
(50) Pan, Q. J.; Wang, Y. M.; Wang, R. X.; Wu, H. Y.; Yang, W. T.; Sun, Z. M.; Zhang, H. X. Bisactinyl halogenated complexes: relativistic density functional theory calculation and experimental synthesis. *RSC Adv.* **2013**, *3*, 1572−1582.
(51) Poojary, M.; Cabeza, A.; Aranda, M. A. G.; Bruque, S.; Clearfield, A. Structure determination of a complex tubular uranyl phenylphosphonate, $(UO_2)_3(HO_3PC_6H_5)_2(O_3PC_6H_5)_2.H_2O$, from

https://dx.doi.org/10.1021/acs.inorgchem.0c02242
Inorg. Chem. 2020, 59, 17028−17037

conventional X-ray powder diffraction data. *Inorg. Chem.* **1996**, *35*, 1468−1473.
(52) Engelter, C.; Knight, C. L.; Thornton, D. A. The infrared and ^{1}H-NMR spectra of 8-hydroxyquinoline adducts of 8-hydroxyquinoline complexes of dioxouranium(VI), thorium(IV) and scandium(III). *Spectrosc. Lett.* **1989**, *22*, 1161−1172.
(53) Sun, J. W.; Baek, J. Y.; Kim, K.-H.; Huh, J.-S.; Kwon, S.-K.; Kim, Y.-H.; Kim, J.-J. Azasiline-based thermally activated delayed fluorescence emitters for blue organic light emitting diode. *J. Mater. Chem. C* **2017**, *5*, 1027−1032.
(54) Huang, J.; Wang, X.; Jacobson, A. J. Hydrothermal synthesis and structures of the new open-framework uranyl silicates $Rb_4(UO_2)_2(Si_8O_{20})$ (USH-2Rb), $Rb_2(UO_2)(Si_2O_6)$ H_2O (USH-4Rb) and $A_2(UO_2)(Si_2O_6)$ $0.5H_2O$ (USH-5A; A = Rb, Cs). *J. Mater. Chem.* **2003**, *13*, 191−196.
(55) Xu, S.; Wang, J.; Liu, S.; Zhao, F.; Xia, H.; Wang, Y. Synthesis, photophysical properties, and computational studies of four-coordinate copper(I) complexes based on benzimidazolylidene N-heterocyclic carbene (NHC) ligands bearing aryl substituents. *J. Mol. Struct.* **2018**, *1153*, 12−19.
(56) Runge, E.; Gross, E. K. Density-Functional Theory for Time-Dependent Systems. *Phys. Rev. Lett.* **1984**, *52*, 997−999.
(57) Uoyama, H.; Goushi, K.; Shizu, K.; Nomura, H.; Adachi, C. Highly efficient organic light-emitting diodes from delayed fluorescence. *Nature* **2012**, *492*, 234−238.
(58) Bideh, B. N.; Roldán-Carmona, C.; Shahroosvand, H.; Nazeeruddin, M. K. Ruthenium phenanthroimidazole complexes for near infrared light-emitting electrochemical cells. *J. Mater. Chem. C* **2016**, *4*, 9674−9679.
(59) Parker, C. A.; Rees, W. T. Correction of fluorescence spectra and measurement of fluorescence quantum efficiency. *Analyst* **1960**, *85*, 587−600.
(60) Zhu, L. J.; Wang, J.; Reng, T. G.; Li, C. Y.; Guo, D. C.; Guo, C. C. Effect of substituent groups of porphyrins on the electroluminescent properties of porphyrin-doped OLED devices. *J. Phys. Org. Chem.* **2010**, *23*, 190−194.
(61) Maji, S.; Kumar, S.; Kalyanasundaram, S. Luminescence studies of uranyl-aliphatic dicarboxylic acid complexes in acetonitrile medium. *Radiochim. Acta* **2020**, *108*, 361−373.
(62) Gorelik, V. S.; Loboiko, A. A.; Bi, D. Photoluminescence spectra of $UO_2(NO_3)_2$. *Inorg. Mater.* **2019**, *55*, 827−833.
(63) Janghouri, M.; Mohajerani, E.; Amini, M. M.; Najafi, E. Red organic light emitting device based on TPP and a new host Material. *Appl. Phys. A: Mater. Sci. Process.* **2014**, *114*, 445−451.
(64) Ma, B.; Kim, B. J.; Deng, L.; Poulsen, D.; Thompson, M. E.; Frechet, J. Bipolar copolymers as host for electroluminescent devices: Effects of molecular structure on film morphology and device performance. *Macromolecules* **2007**, *40*, 8156−8161.
(65) Shahroosvand, H.; Najafi, L.; Mohajerani, E.; Khabbazi, A.; Nasrollahzadeh, M. Green, near-infrared electroluminescence of novel yttrium tetrazole complexes. *J. Mater. Chem. C* **2013**, *1*, 1337−1344.
(66) Shahroosvand, H.; Najafi, L.; Sousaraei, A.; Mohajerani, E.; Janghouri, M. Going from green to red electroluminescence through ancillary ligand substitution in ruthenium(II) tetrazole benzoic acid emitters. *J. Mater. Chem. C* **2013**, *1*, 6970−6980.
(67) Anikeeva, P. O.; Madigan, C. F.; Coe-Sullivan, S. A.; Steckel, J. S.; Bawendi, M. G.; Bulović, V. Photoluminescence of CdSe/ZnS core/shell quantum dots enhanced by energy transfer from a phosphorescent donor. *Chem. Phys. Lett.* **2006**, *424*, 120−125.
(68) Namdas, E. B.; Ruseckas, A.; Samuel, I. D. W.; Lo, S.-C.; Burn, P. L. Triplet exciton diffusion in fac-tris(2-phenylpyridine) iridium-(III)-cored electroluminescent dendrimers. *Appl. Phys. Lett.* **2005**, *86*, 091104.
(69) Fathollahi, M.-R.; Sharifi, M.-J.; Boroumand, F. A.; Raissi, F.; Mohajerani, E. Alternative model for injection-limited current into organic solids. *J. Photonics Energy* **2015**, *5*, 057610.
(70) Fathollahi, M.-R.; Akbari Boroumand, F.; Raissi, F.; Sharifi, M.-J. Quantitative characterization of carrier injection across metal−organic interfaces using Bardeen theory. *Org. Electron.* **2012**, *13*, 905−913.

https://dx.doi.org/10.1021/acs.inorgchem.0c02242
Inorg. Chem. 2020, 59, 17028−17037